

The pre- versus post-main sequence evolutionary phase of B[e] stars

Constraints from ^{13}CO band emission

M. Kraus

Astronomický ústav, Akademie věd České republiky, Fričova 298, 251 65 Ondřejov, Czech Republic
e-mail: kraus@sunstel.asu.cas.cz

Received; accepted

ABSTRACT

Context. Many galactic B[e] stars suffer from improper distance determinations, which make it difficult to distinguish between a pre- and post-main sequence evolutionary phase on the basis of luminosity arguments. In addition, these stars have opaque circumstellar material, obscuring the central star, so that no detailed surface abundance studies can be performed.

Aims. Instead of studying the surface abundances as a tracer of the evolutionary phase, we propose a different indicator for the supergiant status of a B[e] star, based on the enrichment of its circumstellar matter by ^{13}C , and detectable via its ^{13}CO band emission in the K band spectra.

Methods. Based on stellar evolution models, we calculate the variation of the $^{12}\text{C}/^{13}\text{C}$ isotopic surface abundance ratio during the evolution of non-rotating stars with different initial masses. For different values of the $^{12}\text{C}/^{13}\text{C}$ ratio we then compute synthetic first-overtone vibration-rotational band spectra from both the ^{12}CO and ^{13}CO molecule at different spectral resolutions. We further discuss the influence of stellar rotation on the variation of the surface $^{12}\text{C}/^{13}\text{C}$ ratio and on the possibility of ^{13}CO band detection.

Results. The surface $^{12}\text{C}/^{13}\text{C}$ isotope ratio is found to decrease strongly during the post-main sequence evolution of non-rotating stars, from its interstellar value of about 70 to a value of about 15–20 for stars with initial masses higher than $7 M_{\odot}$, and to a value of less than 5 for stars with initial masses higher than $25 M_{\odot}$. We find that detectable ^{13}CO band head emission is produced for isotope ratios $^{12}\text{C}/^{13}\text{C} \lesssim 20$, and can most easily be detected with a spectral resolution of $R \sim 1500 \dots 3000$. For the rotating stellar models, the drop in $^{12}\text{C}/^{13}\text{C}$ already occurs for all stars with $M_{\text{in}} \gtrsim 9 M_{\odot}$ during the main-sequence evolution. The detection of ^{13}CO band head emission in such mid-resolution K band spectra of a B[e] star thus favours an evolved rather than a young nature of the object.

Key words. Stars: early-type – stars: atmospheres – stars: mass-loss – stars: winds, outflows – circumstellar matter

1. Introduction

The classification of B[e] stars according to their evolutionary phase is a long-standing problem. Much effort has been undertaken since Lamers et al. (1998) published the first detailed classification criteria sorting the B[e] stars into the classes of supergiants, Herbig stars, compact planetary nebulae, and symbiotics. Nevertheless, the remaining group of unclassified B[e] stars, which includes about half of all known B[e] stars, has since then gained even more members.

While many targets within the group of unclassified B[e] stars have not been studied yet in detail, there also exists a number of stars showing indications of both a young (Herbig star) as well as an evolved (supergiant star) nature. And one of the reasons for their uncertain classification is their still rather poorly known distance, and hence luminosity (see Table A.1). For a proper assignment of an evolutionary phase to these stars it is, therefore, necessary to find other characteristics that are directly linked to the evolutionary phase of a star as additional classification criteria.

The best studied B[e] supergiant sample is located in the Magellanic Clouds. Their main characteristic is the so-called hybrid character of their spectra, showing indications for both a typical line-driven wind in polar direction, and a slow and low-ionized but high-density wind in the equatorial direction (Zickgraf et al. 1985). Further evidence for non-sphericity of

their winds comes from polarimetric observations, e.g., by Magalhães (1992), Magalhães et al. (2006), and Melgarejo et al. (2001) for the Magellanic Cloud stars, and from, e.g., Zickgraf & Schulte-Ladbeck (1989) for some of the galactic candidates. Detection of molecular emission bands of TiO (Zickgraf et al. 1989) and CO (McGregor et al. 1988, 1989; Morris et al. 1996) in the spectra of several B[e] supergiants confirms the presence of high-density and cool material in the vicinity of these luminous stars.

An additional characteristic of B[e] supergiants is their strong infrared (IR) excess emission (e.g., Zickgraf et al. 1986), indicating that these luminous objects are surrounded by hot or warm dust, whose most probable location is within a massive circumstellar disk. Recent estimates, based on observations with the *Spitzer Space Telescope* Infrared Spectrograph for the Large Magellanic Cloud B[e] supergiant R 126 by Kastner et al. (2006), resulted in a total dust mass within the disk of $\sim 3 \times 10^{-3} M_{\odot}$.

The existence of dusty disks is also one of the major characteristics of Herbig Ae/Be stars (see, e.g., the recent reviews by Waters 2006, and Waters & Waelkens 1998, and references therein). And for many young stellar objects the observations of the CO band heads (Hanson et al. 1997; Bik & Thi 2004; Thi et al. 2005; Bik et al. 2006), although not present in all objects, often resulted in detailed information about the disk structure

and kinematics of the inner disk. A high-density circumstellar disk with molecules and dust is thus a common feature of both the Herbig stars and the B[e] supergiants. The only, and consequently most important difference is the fact that for the Herbig stars the disk material is the remnant of the star formation process.

Since the progenitors of B[e] supergiants must have been massive O-type stars, this close-by dust cannot be pre-main sequence in origin. Any remaining pre-main sequence circumstellar material will have been swept away by the strong radiation pressure of their stellar winds during their main-sequence life-time. The disks around the B[e] supergiants must thus have formed from the wind material itself¹, due to some enhanced mass loss or some violent high-density mass ejection, predominantly within the equatorial regions. Detailed investigations of the UV metallic lines for some Magellanic Cloud B[e] supergiants seen edge-on have revealed terminal disk wind velocities of 60–80 km s⁻¹ only (Zickgraf et al. 1996). They are thus at least a factor of ten lower than the terminal velocities in the polar winds, which show properties similar to those of classical B-type star, i.e., line-driven winds (e.g., Zickgraf et al. 1985). In combination with the enhanced mass fluxes found for the equatorial wind, B[e] supergiants show a density contrast of 100–1000 between the equatorial (i.e. disk) wind and the normal (i.e. polar) wind (Zickgraf et al. 1989). Reasonable attempts at explaining these equatorial flows are provided by the rotationally induced bi-stability mechanism (Lamers & Pauldrach 1991; Pelupessy et al. 2000; Curé 2004; Curé et al. 2005). Even though the formation mechanism is not fully understood and solved yet (see, e.g., Ignace & Gayley 2005; Kraus & Miroshnichenko 2006), the disk-forming winds of the B[e] supergiants must be dense and cool enough to allow for efficient molecule and dust formation.

The most stable molecule is CO, and during their IR spectroscopic studies of early-type emission line stars, McGregor et al. (1988) detected CO band head emission from several targets that later grouped in the unclassified B[e] stars or as B[e] supergiant candidates (see Table A.1).

What remains is the question of where in the disk, i.e., at what distance from the B[e] supergiant star, the CO band emission originates. Recently, Kraus & Borges Fernandes (2005) and Kraus et al. (2006, 2007) have shown that the disks around B[e] supergiants must be predominantly neutral in hydrogen close to the stellar surface in order to reproduce the observed strong [O] emission lines. The temperature in the [O] line forming regions ranges from ~ 8000 K to ~ 6000 K, while the dust must be located further away from the central star, where the disk temperatures dropped below the dust evaporation temperature of 1500 K. CO has a dissociation temperature of about 5000 K. Theoretical CO band calculations have shown that the formation of pronounced band head structures requires a minimum CO temperature of about 2000 K (see, e.g., Kraus 1997 and Sect. 3.1 below). The CO bands, therefore, probe the disk area between the [O] and the dust emission regions. In terms of distance, this temperature argument places the CO formation region beyond the [O] saturation, which usually happens at distances of around 100–300 R_* (see Kraus et al. 2006, 2007).

¹ This argument is only strictly valid if we assume that the B[e] phenomenon is a special phase (for stars with perhaps very specific initial conditions) during single star evolution, which we will assume throughout this paper. If the B[e] phenomenon for these supergiants is caused by some binary interaction or binary merger process, the situation might be completely different.

Since the disks around B[e] supergiants are formed from wind material, we can expect the disk material to mirror the surface composition of the star at the time of ejection. Depending on the evolutionary phase of the star at the time of matter ejection, the disk material already should be enriched in chemically processed material that has been brought to the stellar surface via rotation and mixing processes. Searching for such enhanced abundances within the disk material of B[e] stars might thus provide us with the information necessary to discriminate between a pre- and post-main sequence evolutionary phase of the underlying star.

One of the elements produced during the evolution of massive stars is the carbon isotope ¹³C. Its ratio with the main isotope ¹²C changes drastically during stellar evolution, making ¹³C an ideal tracer for post-main sequence evolutionary phases. We already know of the existence of ¹²CO band emission from the disks of B[e] supergiants, but none of the targets has been reported to show ¹³CO emission so far. The reason for this is certainly the fact that either the spectral resolution used was generally too low ($R \lesssim 500$, see Sect. 3), or, when using high-resolution spectrographs, the spectral region covered by the observations were restricted to the region around the first ¹²CO bandhead only, which does not include the range of ¹³CO emission. This paper, therefore, investigates the possible appearance of ¹³CO band head emission during the evolution of OB stars, based on theoretical model calculations of the first-overtone bands of ¹²CO and ¹³CO in the K band spectra.

The paper is structured as follows: In Sect. 2 we study the variation of the ¹²C/¹³C surface abundance ratio during the evolution of predominantly massive stars. Next, we calculate simple synthetic CO first-overtone band spectra in Sect. 3 of the CO molecule² and discuss the appearance of the band heads of the ¹³CO molecule as a function of ¹²C/¹³C ratio as well as of spectral resolution. In Sect. 4 we discuss the reliability of our calculations and applicability to the B[e] supergiants, before we summarise our results in Sect. 5.

2. Variation of the ¹³C surface abundance during stellar evolution of massive stars

During the evolution of massive stars, heavy elements produced during the different burning processes are brought to the stellar surface via rotation and mixing processes (see, e.g., the reviews by Pinsonneault 1997 and Maeder & Meynet 2000). The surface abundances of individual elements will thus change with time. Due to the (high) mass loss of massive stars via line-driven winds, these changes in surface abundances will thus translate into abundance changes in the wind, which then clearly shows the presence of chemically enriched, processed material. Studies of the chemical composition of the wind (or more generally: of the circumstellar) material of post-main sequence evolutionary phases of massive stars are, therefore, ideal to determine the evolutionary phase of the central star.

To study the changes in surface abundances (and hence of the wind abundances), we use the grid of Schaller et al. (1992) for non-rotating stars at solar metallicity. In Fig. 1 we plot the changes in surface abundances along the evolutionary tracks (indicated by the grid numbers) of ¹²C, ¹³C, ¹⁴N, and ¹⁶O with respect to the surface hydrogen abundance at the same grid point. The ratios have been calculated from the mass fractions provided

² Note that by writing CO without indication of the isotope, we always refer to the main isotope, i.e., the ¹²CO molecule.

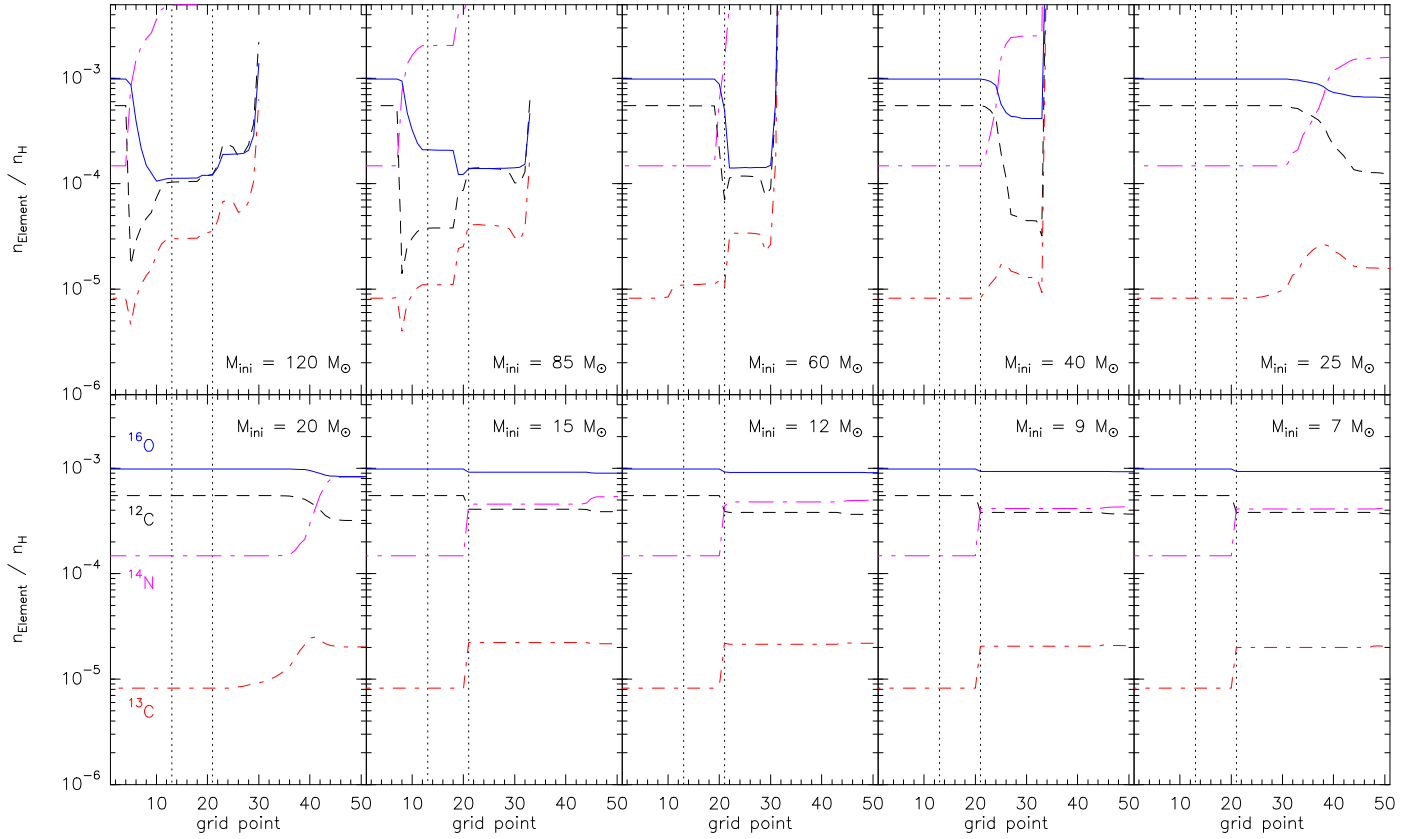


Fig. 1. Changes in ^{12}C , ^{13}C , ^{14}N , and ^{16}O surface abundances with respect to the hydrogen surface abundance along the evolutionary tracks of non-rotating stars, as indicated by the grid points. The ratios were calculated from the data of Schaller et al. (1992) for solar metallicity. The approximate end of the core H burning and the onset of the core He burning phases are indicated by the two vertical dotted lines in each panel.

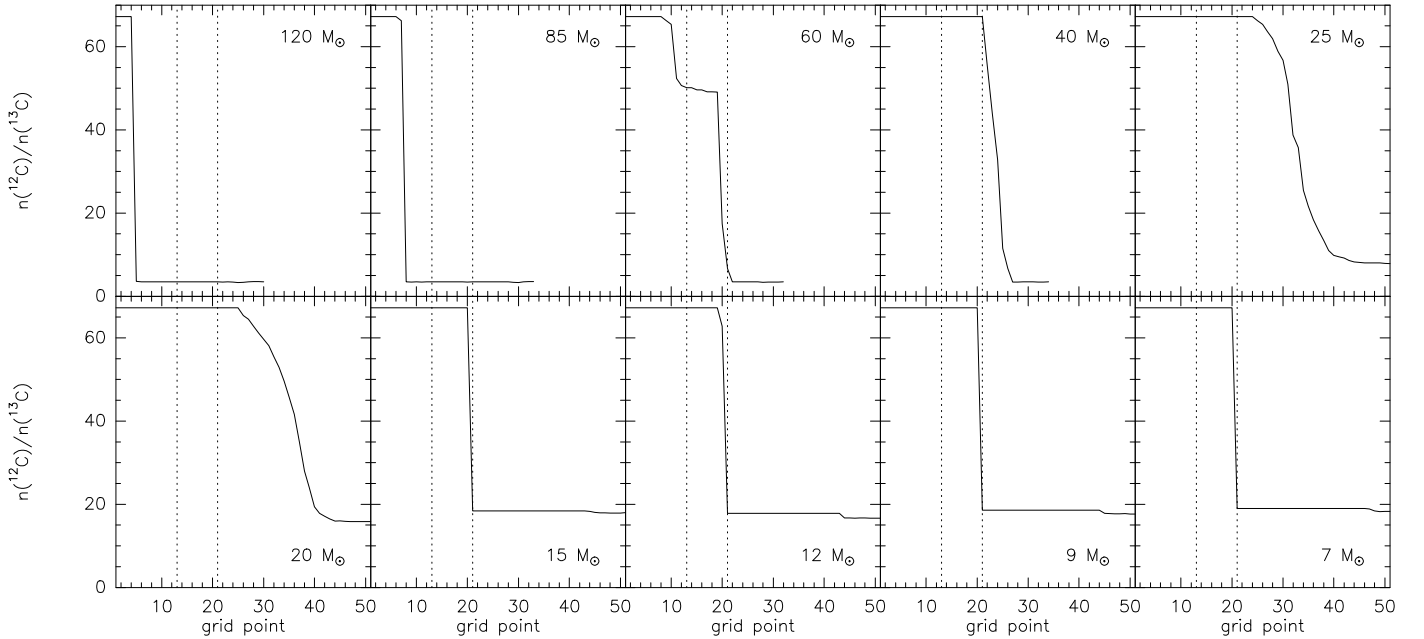


Fig. 2. Change of the $^{12}\text{C}/^{13}\text{C}$ surface abundance ratio during stellar evolution of non-rotating massive stars at solar metallicity. The ratios are calculated from the tables of Schaller et al. (1992). The dotted lines have the same meaning as in Fig. 1.

in the data files of Schaller et al. (1992). The grid points that indicate the approximate end of the core H burning and the onset of the core He burning phases are indicated by the two vertical dotted lines in each panel. The abundance curves for stars with

initial masses $M_{\text{ini}} > 40 M_{\odot}$ stop around grid point ~ 30 (i.e. before the end of core He burning) since these stars have lost their complete outer hydrogen shell via strong mass loss.

The change in chemical surface composition during the main-sequence lifetime is quite obvious for the most massive stars, while the surface abundances of the less massive stars remain at their initial values until the onset of core He burning or even longer. The elements with clearly increasing abundances during the evolution are ^{14}N and ^{13}C , while at the same time the abundances of ^{16}O and ^{12}C slightly decrease. The nitrogen enrichment of the surface (and hence the wind) material is usually used as an indicator to trace evolved evolutionary phases of massive stars, as for the classical OB supergiants (see, e.g., Crowther et al. 2002; Hillier et al. 2003; Evans et al. 2004; Searle et al. 2008) or the Luminous Blue Variables (e.g., Lamers et al. 2001).

The direct study and comparison of the surface abundances of the B[e] stars would be an ideal tool for the determination of their evolutionary phases. Unfortunately, due to their usually high density circumstellar material (caused by high mass loss in the case of B[e] supergiants), their spectra are often crowded with pure emission lines, and the photosphere of most targets is not visible at all. A direct way to measure their surface abundances is thus not possible. The only way to draw conclusions about their surface composition is to study the chemical abundances from their emission lines formed within their close-by circumstellar material. However, to determine the CNO abundances of B[e] stars from their emission lines, it is necessary to have a detailed description of the exact geometry, the inclination angle of the system, and the latitude dependent ionization structure. This information is usually not available and can hardly be derived from the modeling of the emission lines alone. We therefore need another, more reliable indicator for the evolutionary state of an individual object.

One important indicator of post-main sequence evolutionary phases is the surface abundance of the isotope ^{13}C , or more precisely, the change in the isotopic ratio $^{12}\text{C}/^{13}\text{C}$. The strong increase in ^{13}C in combination with the (slight) decrease in ^{12}C surface abundances (see Fig. 1) results in a rather steep decrease of the $^{12}\text{C}/^{13}\text{C}$ ratio from its initial interstellar value of ~ 70 to values < 20 for stars with initial masses $\lesssim 40 M_{\odot}$, and for stars with initial masses $\geq 60 M_{\odot}$ even to $^{12}\text{C}/^{13}\text{C} \lesssim 5$. The variation in the $^{12}\text{C}/^{13}\text{C}$ surface abundance ratio during the evolution of massive stars at different metallicity is depicted in Fig. 2.

With an abundance ratio lower than about 20, the ^{13}C isotope should be easily detectable. However, our intention is not to search for individual emission lines of the ^{13}C atom, but rather to concentrate on the molecular emission of CO and its ^{13}CO isotope. Besides, our investigations will be restricted to the ^{12}CO and ^{13}CO , only, since the abundances in ^{17}O and ^{18}O compared to the main isotope ^{16}O are generally extremely low, even during the late evolutionary phases of massive stars. Contributions from the C^{17}O and C^{18}O isotopes to the total CO band structures are thus negligible.

3. CO band formation

CO first-overtone band emission is a well known feature arising especially from the rotating accretion disks around young stellar objects (YSO), and the physics of CO band formation in such rotating pre-main sequence disks has already been discussed widely in the literature (see, e.g., Scoville et al. 1980; Carr 1989; Najita et al. 1996; Kraus 2000; Kraus et al. 2000). The main focus in YSO research is therefore especially the structure of the $2 \rightarrow 0$ band head, which contains the complete velocity information, and from which the rotation velocity, disk inclination, as well as some information concerning the density and temperature within the CO forming disk region can be derived (e.g.,

Carr et al. 1993; Chandler et al. 1993; Carr 1995; Najita et al. 1996; Kraus 2000; Kraus et al. 2000; Bik & Thi 2004; Berthoud et al. 2007).

Such high-resolution $2 \rightarrow 0$ band head observations also would be very important for B[e] stars in studying the kinematics of the CO gas, especially for the discrimination between whether the disks around B[e] supergiants are Keplerian rotating (i.e., stable, long-lived disks), or outflowing disk-forming winds (see, e.g., Porter 2003; Kraus et al. 2007). For our purpose related to the B[e] supergiants' evolutionary phase, however, we need to study a much larger (in wavelength) portion of the complete CO first-overtone band structures, because we want to find out (i) where in the K band spectra of B[e] supergiants we can expect the ^{13}CO band heads to show up, (ii) during which evolutionary phases observable ^{13}CO band head emission might be generated, and (iii) what the most suitable spectral resolution is to easily detect these ^{13}CO band heads.

3.1. Synthetic band spectra of ^{12}CO

For the calculation of the CO band spectra, we follow the description of Kraus et al. (2000). Due to the lack of knowledge of the proper shape and structure of the B[e] supergiant stars' disks, we keep the calculations simple, assuming the CO gas to be isothermal. We further assume that the CO gas is in local thermodynamic equilibrium. Then, the emission at frequency ν is simply given by

$$I_{\nu} = B_{\nu}(T_{\text{CO}})(1 - e^{-\tau_{\nu}}) \quad (1)$$

with the optical depth

$$\tau_{\nu} = \kappa_{\nu,^{12}\text{CO}} N_{^{12}\text{CO}}. \quad (2)$$

Here, $\kappa_{\nu,^{12}\text{CO}}$ is the absorption coefficient per ^{12}CO molecule, and $N_{^{12}\text{CO}}$ is the column density of the ^{12}CO gas for which we adopt a value of 10^{17} cm^{-2} in order to keep the emission optically thin at all wavelengths over the complete band spectrum. We take into account a total of 10 vibration bands, and within each vibration band a total of 140 rotation levels. The so-called Dunham coefficients to calculate the energy levels are taken from Farrenq et al. (1991), and the Einstein coefficients for spontaneous emission from Chandra et al. (1996).

To calculate $\kappa_{\nu,^{12}\text{CO}}$, we need to specify the profile function of the individual vibration-rotational lines for which we use, for simplicity, a Gaussian profile. The width of the Gaussian we describe by a fixed (internal) CO velocity of 30 km s^{-1} . The choice of this velocity is not crucial, unless the internal velocity exceeds the one given by the spectral resolution. For some first test calculations, we smear the CO band spectra to an arbitrary spectral resolution of $R = 1500$, corresponding to a velocity resolution of about 200 km s^{-1} .

To study the variation in the individual band head peak intensities, we calculate the structure of the first-overtone bands for different CO temperatures, ranging from 1000 K to 5000 K. The results are shown in Fig. 3 with the positions of the band edges³ indicated by the ticks in the top panel. The formation of clear band heads starts for temperatures $T_{\text{CO}} \gtrsim 2000 \text{ K}$, while for CO temperatures below 2000 K no individual and clearly identifiable band heads emerge. For $T_{\text{CO}} \approx 1000 \text{ K}$ only the levels within the first vibrational band are excited, giving rise to the

³ For clarification, we use the terminus *band head* when talking about the intensity peaks, while the transition of lowest wavelength in each band we call the *band edge*.

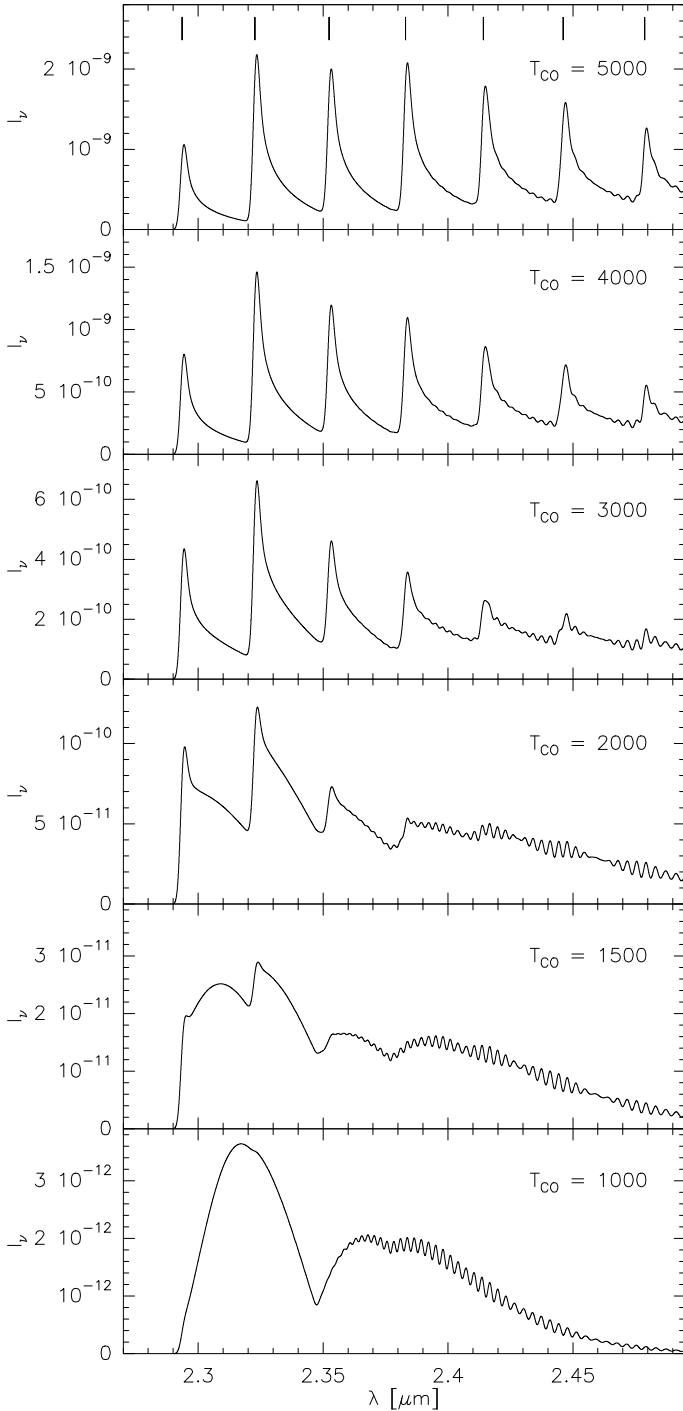


Fig. 3. Influence of the temperature on the synthetic ^{12}CO band emission spectra. Clear band head structures form for $T_{\text{CO}} \geq 2000$ K.

broad, double emission feature. The higher the temperature, the more vibrational bands can be excited and the more individual band heads appear. A further effect of increasing CO temperature is the strong increase in band head intensities, with the $3 \rightarrow 1$ as the clearly dominating one, while the $2 \rightarrow 0$ band head becomes depressed with increasing temperature due to depopulation into the higher vibrational levels. Due to this strong intensity increase with CO temperature, most of the observable band head emission originates from the hottest CO gas, i.e., from the disk regions closest to the star.

3.2. The appearance of the ^{13}CO bands

The slightly higher mass of the ^{13}C isotope has two consequences for the energy levels within the diatomic molecule: (i) A higher mass results in a higher moment of inertia, reducing the energy of the individual rotational levels within each vibrational band. (ii) Since the frequencies of the vibrations depend on the reduced mass only, the vibrational energy levels within the more massive ^{13}CO isotope will all be reduced compared to those within the ^{12}CO molecule. Consequently, the net effect of the higher mass of the isotope is a shift of the coupled vibration-rotational transitions, and hence of the complete band spectrum, to longer wavelengths. Since the wavelength shift (i.e., the reduction in energy) is especially strong for the vibrational transitions, a clear wavelength separation appears between the bands of ^{12}CO and ^{13}CO . The lowest band edge of the first-overtone bands arises at $2.3448\ \mu\text{m}$ ($2 \rightarrow 0$), i.e., at a wavelength between the second and third band edge of the ^{12}CO bands. This fact is of major importance for the identification of the ^{13}CO band heads in the total spectrum.

Since the main effect of the different masses is a shift of the individual vibration-rotational lines to higher wavelengths, the bands of the ^{13}CO molecule will, in general, have a very similar shape to those of ^{12}CO . To compute the total band spectrum consisting of the ^{12}CO and ^{13}CO transitions, we again calculate the intensity, I_ν , at each wavelength with Eq. (1), but for the optical depth, τ_ν , we now need to include the contribution of the ^{13}CO molecule into Eq. (2), giving

$$\tau_\nu = \kappa_{\nu,^{12}\text{CO}} N_{^{12}\text{CO}} + \kappa_{\nu,^{13}\text{CO}} N_{^{13}\text{CO}}, \quad (3)$$

where $N_{^{13}\text{CO}}$ and $\kappa_{\nu,^{13}\text{CO}}$ are the column density and the absorption coefficient per ^{13}CO molecule, respectively.

It is convenient to parametrize the column density of the isotope, $N_{^{13}\text{CO}}$, in terms of $N_{^{12}\text{CO}}$ and the carbon isotope abundance ratio, $n_{^{12}\text{C}}/n_{^{13}\text{C}}$, for which we assume that it equally translates into the CO isotope ratio, so that we can write

$$N_{^{13}\text{CO}} = \frac{N_{^{13}\text{CO}}}{N_{^{12}\text{CO}}} N_{^{12}\text{CO}} = \frac{n_{^{13}\text{CO}}}{n_{^{12}\text{CO}}} N_{^{12}\text{CO}} = \frac{N_{^{12}\text{CO}}}{n_{^{12}\text{C}}/n_{^{13}\text{C}}}, \quad (4)$$

with the carbon isotope abundance ratio, $n_{^{12}\text{C}}/n_{^{13}\text{C}}$, as the only free parameter. From this relation it is already obvious that the emergence of the ^{13}CO bands strongly depends on the carbon isotopic ratio, i.e., the lower this ratio, the higher the probability of ^{13}CO band appearance.

In our test calculations we use the following values for the $n_{^{12}\text{C}}/n_{^{13}\text{C}}$ abundance ratio: 70, 15, 10, and 5. While the first value approximately represents the interstellar (i.e., initial) ratio, the latter appear during the more interesting, later evolutionary stages of stars with different initial masses (see Fig. 2). The emerging total spectra for these four ratios and for different spectral resolutions are displayed in Fig. 4, with the wavelengths of both, the ^{12}CO and ^{13}CO band edges, indicated in the top panels.

For an interstellar carbon isotopic ratio of 70, the ^{13}CO bands remain undetectable. The first indications for ^{13}CO band heads peaking out of the total CO spectrum are for an isotopic ratio of 15, while for even lower ratios, the individual ^{13}CO band heads are clearly present. However, the appearance of these band heads strongly depends on the chosen spectral resolution. To show the effect of spectral resolution, we calculated synthetic CO bands for increasing resolution, from $R = 500$, which corresponds approximately to the value used by McGregor et al. (1988) as was discussed in Sect. 1, to $R = 5000$, with the intrinsic CO velocity fixed at $30\ \text{km s}^{-1}$. While for the lowest resolution the ^{13}CO band heads are not visible at all, their smooth structure breaks down at

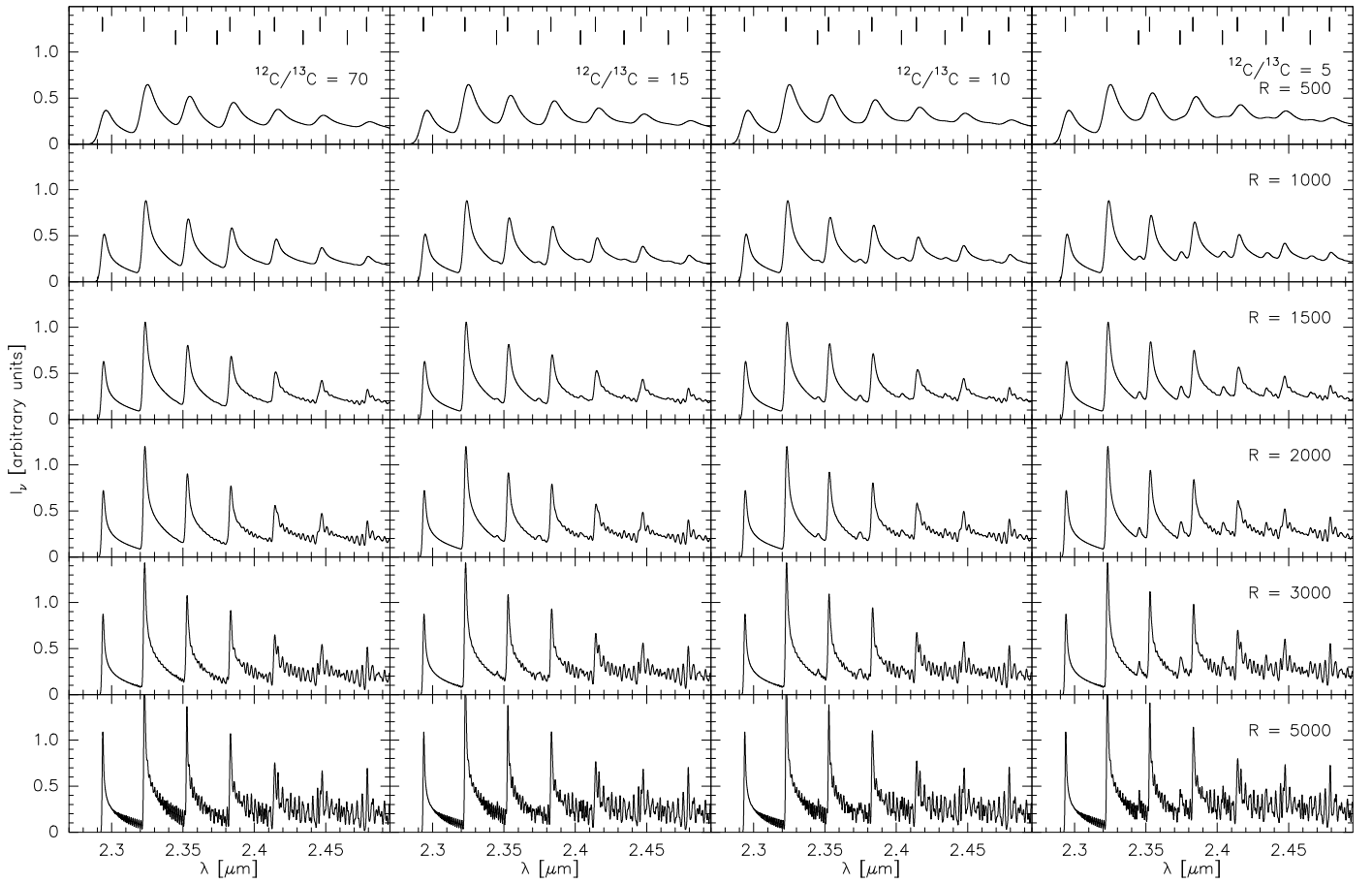


Fig. 4. Synthetic, optically thin ^{12}CO plus ^{13}CO first-overtone band spectra computed for $T_{\text{CO}} = 3500$ K. The individual panels are for increasing spectral resolutions (from top to bottom) and for decreasing $^{12}\text{C}/^{13}\text{C}$ ratios (from left to right).

the chosen highest resolution, since at high resolution we start to resolve individual vibration-rotational lines. The most suitable range in resolution that follows from these calculations is thus between $R = 1000$ and $R = 3000$.

The terminal velocity of the equatorial winds in B[e] supergiants was found to be $\lesssim 80 \text{ km s}^{-1}$ (Zickgraf et al. 1996), so that for edge-on systems a resolution as high as $R = 5000$ would also still deliver smooth ^{13}CO band heads. However, since not much is known about the possible inclinations of the galactic B[e] supergiant candidates, a lower resolution ($R \lesssim 3000$) is preferable for the detection of smooth ^{13}CO band heads.

3.3. Influence of optical depth effects

Besides the CO temperature, the column density of the emitting region is a further important parameter that triggers the intensity (and thus the observability) of the CO bands. In this section, we therefore briefly discuss the influence of the CO column density, and hence of the optical depth, on the global appearance of the CO bands and, especially, on the appearance of the ^{13}CO band heads.

We calculate the CO bands for a fixed temperature of $T_{\text{CO}} = 3500$ K and carbon isotopic ratio of $^{12}\text{C}/^{13}\text{C} = 5$ and for increasing ^{12}CO column densities. The results for three different values of the column density are shown in Fig. 5. Contrary to the mid and top panel, which show clear indications for partially optically thick emission, the chosen column density in the bottom

panel is low enough to guarantee that the CO bands are still optically thin throughout the spectrum.

The influence of the increasing optical depth becomes obvious in the strong increase of the CO "quasi-continuum", starting especially at long wavelengths, which leads to a reduction of the ratio between the peak and the inter-peak (i.e., the quasi-continuum) intensity. An additional optical depth effect is the broadening of the band heads on their long-wavelength "wing". Nevertheless, the ^{13}CO band heads remain detectable, even for significant optical depth values within the ^{12}CO bands.

4. Discussion

The rising of the ^{13}CO band heads with decreasing carbon isotopic ratio is nicely displayed in Fig. 4. Since the decrease in isotopic ratio is a clear indicator of stellar evolution (see Fig. 2 and Sect. 2), we can claim that, if ^{13}CO band head emission is identified within the K band spectra of a massive star, it hints at an evolved nature of the object. Whether and how this can be used to solve the problem of the evolutionary phase of the B[e] supergiants, or B[e] stars in general, is discussed in the following.

4.1. Comparison with non-rotating stellar evolution models

For a sense of whether the B[e] supergiant candidates in Table A.1 will show ^{13}CO bands in their K band spectra at all, we need to specify those evolutionary phases with suitably low

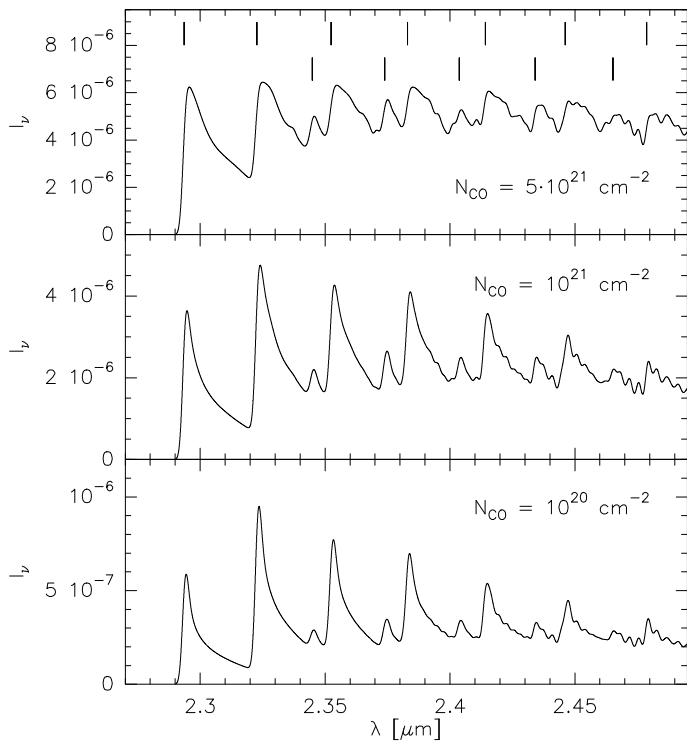


Fig. 5. CO Band structure for increasing CO column density (from bottom to top), i.e., increasing optical thickness.

isotopic ratio and compare them with the locations of the B[e] stars within the HR diagram. Such a comparison is performed in the left panel of Fig. 6, where we plot the stellar evolutionary tracks from Schaller et al. (1992) for non-rotating stars at solar metallicity. Those evolutionary phases during which the $^{12}\text{C}/^{13}\text{C}$ ratio drops below $\lesssim 20$ and further below $\lesssim 15$ are indicated. Also included are the positions (with error bars) of the galactic B[e] supergiant candidate sample.

Obviously, only the evolutionary tracks for stars with highest initial mass (i.e., $M_{\text{in}} \gtrsim 40 M_{\odot}$) show an overlap of their evolutionary phases of low carbon isotopic ratio with the positions of the most luminous B[e] supergiant candidates. For these targets, the detection of ^{13}CO bands would immediately classify these as B[e] supergiants, and for stars in the mass range $40 M_{\odot} \lesssim M_{\text{in}} \lesssim 60 M_{\odot}$, even constrain the B[e] supergiant phase to late evolutionary phases, i.e., within the second blue supergiant phase during the evolution.

Stellar models with $M_{\text{in}} < 15 M_{\odot}$ reach a carbon isotopic ratio of about 15–20 during their evolution along the blue loop. Even though there exist some B[e] stars within this mass range, the $^{12}\text{C}/^{13}\text{C}$ ratio for these stars might not be low enough for a definite ^{13}CO band detection in low resolution. For these stars, a high-resolution high signal-to-noise spectrum covering the region around the $2 \rightarrow 0$ ^{13}CO band head might be more suitable to search for (and resolve) individual vibration-rotation lines.

For the stellar models of intermediate mass stars ($15 M_{\odot} \lesssim M_{\text{in}} \lesssim 40 M_{\odot}$), the $^{12}\text{C}/^{13}\text{C}$ ratio changes only at the end of their evolution, i.e. within the red part of the HR diagram. For this mass range thus there exists no overlap of the low carbon isotopic ratio regime with the locations of the B[e] supergiant candidates.

4.2. The influence of stellar rotation

It is generally assumed that the disk formation around B[e] supergiants is linked to rapid rotation of the central stars. In fact, for 4 Magellanic Cloud B[e] supergiants, projected stellar rotation values (i.e., $v \sin i$) could be determined. These stars indeed seem to rotate at a significant fraction of their critical velocity (Gummersbach et al. 1995; Zickgraf 2000, 2006; Kraus et al. 2008). Whether all B[e] supergiants are rapid rotators, is, however, not known and difficult to determine, since for the rest of the targets no photospheric absorption lines can be detected due to their high-density winds.

To date, nothing is known about possible rotation velocities of the galactic B[e] supergiant candidates. Nevertheless, we investigated the influence of stellar rotation on the variation of the surface $^{12}\text{C}/^{13}\text{C}$ isotope ratio. For this, we used the tables of Meynet & Maeder (2003) for rotating stars at solar metallicity. The evolutionary tracks are shown in the right panel of Fig. 6, and the evolutionary phases with $20 \geq ^{12}\text{C}/^{13}\text{C} \geq 15$ and $^{12}\text{C}/^{13}\text{C} \leq 15$ are again indicated. The general trend of the stellar rotation is to enhance the stellar surface abundance with ^{13}C much earlier during the stellar evolution. And interestingly, for the rotating models the $^{12}\text{C}/^{13}\text{C}$ isotope ratio drops below a value of 20 already during the main-sequence evolution of even the stars with lowest (i.e., here $9 M_{\odot}$) initial mass, and even stars with an initial mass of $25 M_{\odot}$ experience a decrease in isotope ratio to $^{12}\text{C}/^{13}\text{C} \leq 15$ during their late evolutionary phase. In the presence of stellar rotation, the positions of all our B[e] supergiant candidates thus fall into regions with decreased $^{12}\text{C}/^{13}\text{C}$ isotope ratio. The search for ^{13}CO band emission, therefore, seems to be a promising way to distinguish between pre- and post-main sequence evolution of B[e] stars.

4.3. The B[e] supergiant candidate GG Car

In Fig. 6 we emphasized the position of the B[e] supergiant candidate GG Car based on the stellar parameter determinations of earlier investigations by McGregor et al. (1988) and Lopes et al. (1992). According to these studies, it seems that GG Car has evolved from a progenitor star of $M_{\text{in}} \simeq 15 \dots 22 M_{\odot}$.

Recently, Domiciano de Souza et al. (in preparation) performed VLTI/AMBER observations of GG Car and extracted its K band spectrum. Interestingly, the AMBER spectrum of GG Car, which has a spectral resolution of $R \sim 1500$, seems to display clearly detectable ^{13}CO band emission (Chesneau & Domiciano de Souza, private com.), classifying GG Car as a B[e] supergiant star. Based on the peak/inter-peak intensity ratio, the CO emission seems to be rather optically thin, and the detected strength of the ^{13}CO band heads speaks in favour of a $^{12}\text{C}/^{13}\text{C}$ isotope ratio of the order of $\lesssim 10$. Such a low ratio is, however, not expected within the suspected evolutionary phase of GG Car, neither from the non-rotating, nor from the rotating stellar evolution models. This discrepancy might indicate that either the luminosity of GG Car (and hence its initial mass) has been considerably underestimated, or its progenitor star must perhaps have been rotating much faster than 300 km s^{-1} , resulting in a much stronger ^{13}C surface abundance enhancement than the predictions from the rotating models of Meynet & Maeder (2003). In any case, the detection of the unexpectedly strong ^{13}CO band heads in GG Car needs to be studied in more detail, including a careful modeling of the ^{12}CO and ^{13}CO band emission (Domiciano de Souza et al., in preparation). In addition, more interferometric studies to spatially resolve the CO bands,

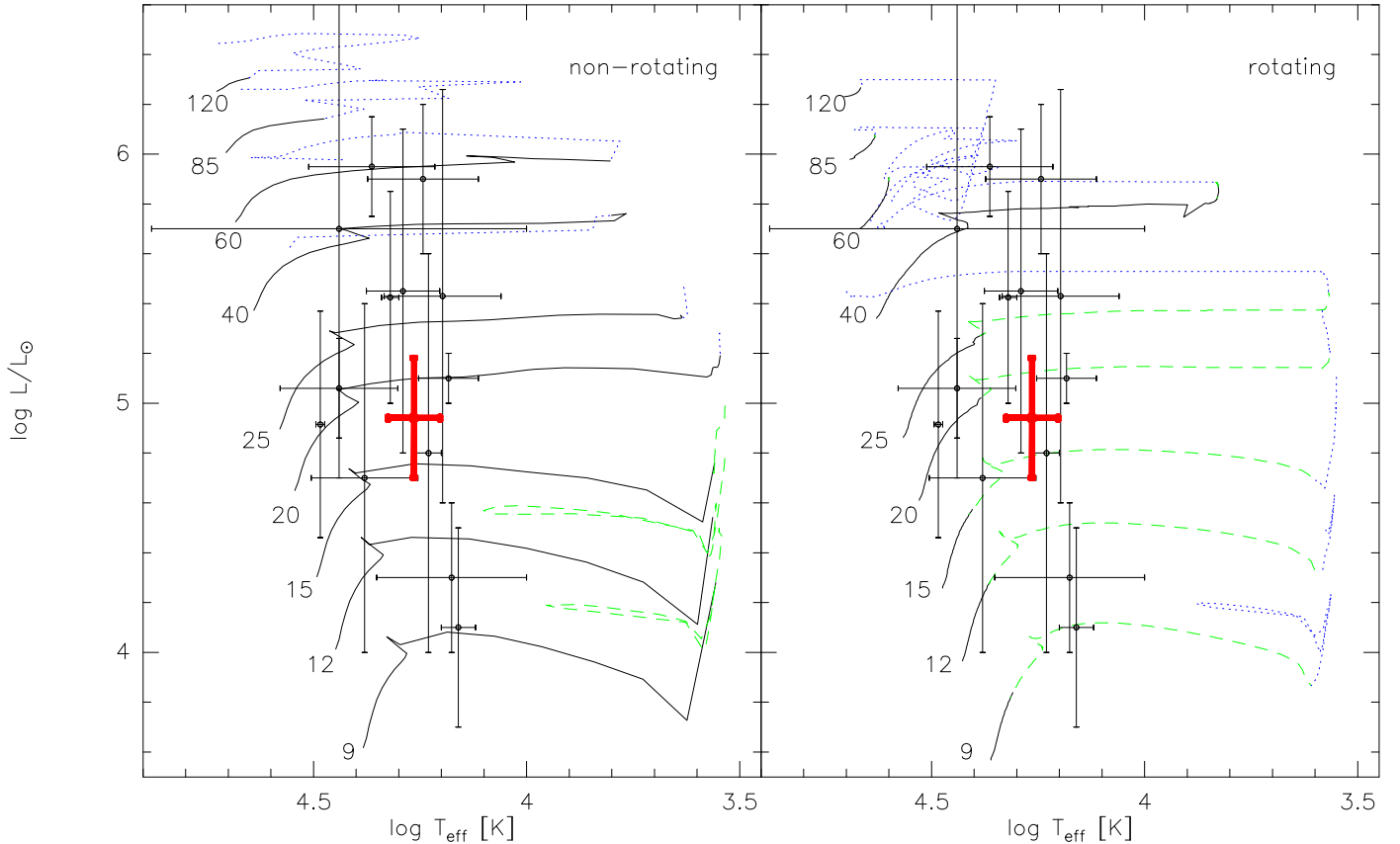


Fig. 6. Comparison of the positions of the galactic B[e] supergiant candidates from Table A.1 with evolutionary tracks of non-rotating (left panel, from Schaller et al. 1992) and rotating (right panel, from Meynet & Maeder 2003) stellar evolutionary models at solar metallicity. The dashed and dotted parts of the tracks indicate those evolutionary phases with $20 \geq {}^{12}\text{C}/{}^{13}\text{C} \geq 15$ and ${}^{12}\text{C}/{}^{13}\text{C} \leq 15$, respectively. The position of GG Car is emphasized.

as has recently been shown by Tatulli et al. (2008), are definitely needed.

5. Conclusions

For many galactic B[e] stars it is not clear whether they are pre-main sequence stars (i.e., Herbig stars) or whether they belong to the group of B[e] supergiants. The main reason for this long-standing problem in classification is their often only poorly known distance, resulting in huge errorbars for the stellar luminosities. In addition, these stars usually have high density circumstellar material obscuring the stellar photosphere, so that an abundance study of their chemical surface composition is not possible.

To overcome these problems, we suggest a different way to distinguish between the pre- and post-main sequence evolutionary phase of the individual targets based on the increasing ${}^{13}\text{C}$ abundance on the stellar surface at post-main sequence evolutionary phases, and hence an increased ${}^{13}\text{C}$ abundance in the winds of the supergiant stars. Since typical B[e] supergiants (such as those in the Magellanic Clouds) show the presence of CO band emission arising in their high-density, neutral circumstellar disks, we investigate the conditions under which observable ${}^{13}\text{CO}$ band emission in the K band spectra of B[e] supergiant candidates is generated. Only stars for which the ${}^{12}\text{C}/{}^{13}\text{C}$ isotope ratio on the stellar surface (and hence in the wind material) has dropped substantially, from the initial, interstellar value of about 70 to less than 20, are found to be suitable to produce

observable ${}^{13}\text{CO}$ band emission. Such a drop in isotope ratio happens naturally in the post-main sequence evolution of extremely massive stars, for which mixing processes and the loss of the outer shells via strong mass loss result in a strong increase in ${}^{13}\text{C}$ surface abundance. In the case of rotating stellar models, this surface enrichment in the ${}^{13}\text{C}$ isotope is much more efficient so that even stars with moderate initial mass (i.e., stars with $M_{\text{in}} \geq 9 M_{\odot}$) already show considerable variations, i.e., a drop in the ${}^{12}\text{C}/{}^{13}\text{C}$ isotope ratio. The computation of synthetic emission spectra of both the ${}^{12}\text{CO}$ and ${}^{13}\text{CO}$ bands for different resolutions revealed that a spectral resolution of $R \sim 1500 \dots 3000$ is ideal for the detection of the ${}^{13}\text{CO}$ band heads.

Interestingly, the B[e] supergiant candidate GG Car has recently been found to show ${}^{13}\text{CO}$ band emission, classifying it definitely as a B[e] supergiant. The observed strength of its ${}^{13}\text{CO}$ bands is, however, in disagreement with the model predictions for its postulated position within the HR diagram, meaning that either its luminosity and initial mass have been considerably underestimated, or its progenitor star must have been rotating much faster than the 300 km s^{-1} used in the rotating stellar evolution models. And also for the B[e] supergiant candidate CPD-57°2874 some tentative ${}^{13}\text{CO}$ detection has been reported (Chesneau & Domiciano de Souza, private com.), indicating that the search for and detection of ${}^{13}\text{CO}$ bands is indeed an ideal tool to discriminate between the pre- and post-main sequence evolutionary phase for the still large number of unclassified B[e] stars.

Table A.1. Parameters of galactic B[e] supergiant candidates. For each object we provide the ranges in luminosity and temperature as found in the literature. We further indicate for each target whether CO band emission has been detected in their *K* band spectra. A question mark means that no CO band emission was detected for $R \sim 450$.

Object	$\log L/L_{\odot}$	T_{eff} [K]	Ref.	<i>K</i> band spectra	^{12}CO	Ref.
CD-42°11721	4.0 ± 0.3 > 4.5	13–15 000 16 000	Borges Fernandes et al. (2007) McGregor et al. (1988)	yes	?	McGregor et al. (1988)
CPD-52°9243	5.9 5.45 ± 0.25 5.4	16 200 13–22 000 16 000	Lopes et al. (1992) Winkler & Wolf (1989) McGregor et al. (1988)	yes	yes	McGregor et al. (1988)
CPD-57°2874	> 4.8 5.7 ± 0.4	16 000 17–23 000	McGregor et al. (1988) Domiciano de Souza et al. (2007)	yes	yes	McGregor et al. (1988); Domiciano de Souza et al. (in prep.)
GG Car	4.7 5.18	16 000 20 800	McGregor et al. (1988) Lopes et al. (1992)	yes	yes	McGregor et al. (1988); Morris et al. (1996); Domiciano de Souza et al. (in prep.)
Hen 3-298	5.1 ± 0.3	13–17 500	Miroshnichenko et al. (2005)	yes	yes	Miroshnichenko et al. (2005)
Hen 3-303	4.3 ± 0.3	10–20 000	Miroshnichenko et al. (2005)	yes	no	Miroshnichenko et al. (2005)
HD 87643	4.9 5.46 4.0–5.6	16 000 16 200 17–18 000	McGregor et al. (1988) Lopes et al. (1992) Oudmaijer et al. (1998)	yes	?	McGregor et al. (1988)
MWC 84	< 4.0 5.4	18–22 000 18–30 000	Miroshnichenko et al. (2002) Hynes et al. (2002)			
MWC 137	4.46 5.37	31 000 30 000	Hillenbrand et al. (1992) Esteban & Fernández (1998)			
MWC 300	5.7–5.85 5.1 ± 0.1	20–22 000 ~ 20 000	Wolf & Stahl (1985) Miroshnichenko et al. (2004)			
MWC 314	5.95 ± 0.2	16 400–29 700	Miroshnichenko et al. (1998)			
MWC 349 A	5.7 ± 1.0 6.1 ± 0.1	20–28 000 32–35 000	Hofmann et al. (2002) Hartmann et al. (1980)	yes	yes	Geballe & Persson (1987); Kraus et al. (2000)
MWC 873	6.26 5.0 ± 0.4 6.0	13 000 20 000 11 500	Lopes et al. (1992) Miroshnichenko et al. (2003) Machado et al. (2003)	yes	yes	McGregor et al. (1988)
W9 (Ara C)	4.86–5.26	20–35 000	Clark et al. (1998)			

Appendix A: Galactic B[e] supergiant candidates

Table A.1 contains a list of the currently known galactic B[e] supergiant candidates.

Acknowledgements. I am grateful to Olivier Chesneau, Armando Domiciano de Souza, and Marcelo Borges Fernandes for exciting discussions on ^{13}CO band head observations with VLT/AMBER, and to the anonymous referee for helpful comments. This research made use of the NASA Astrophysics Data System (ADS) and of the SIMBAD database. I gratefully acknowledge financial support from GA AV ČR, under grant number KJB300030701.

References

- Berthoud, M. G., Keller, L. D., Herter, T. L., Richter, M. J., & Whelan, D. G. 2007, *ApJ*, 660, 461
- Bik, A., & Thi, W. F. 2004, *A&A*, 427, L 13
- Bik, A., Kaper, L., & Waters, L. B. F. M. 2006, *A&A*, 455, 561
- Borges Fernandes, M., Kraus, M., Lorenz Martins, S., & de Araújo, F. X. 2007, *MNRAS*, 377, 1343
- Carr, J. S. 1989, *ApJ*, 345, 522
- Carr, J. S. 1995, *Ap&SS*, 224, 25
- Carr, J. S., Tokunaga, A. T., Najita, J., Shu, F., & Glassgold, A. E. 1993, *ApJ*, 411, L 37
- Chandler, C. J., Carlstrom, J. E., Scoville, N. Z., Dent, W. R. F., & Geballe, T. R. 1993, *ApJ*, 412, L 71
- Chandra, S., Maheshwari, V. U., & Sharma, A. K. 1996, *A&AS*, 117, 557
- Clark, J. S., Fender, R. P., Waters, L. B. F. M., et al. 1998, *MNRAS*, 299, L 43
- Crowther, P. A., Hillier, D. J., Evans, C. J., et al. 2002, *ApJ*, 579, 774
- Curé, M. 2004, *ApJ*, 614, 929
- Curé, M., Rial, D.F., & Cidale, L. 2005, *A&A*, 437, 929
- Domiciano de Souza, A., Driebe, T., Chesneau, O., et al. 2007, *A&A*, 464, 81
- Evans, C. J., Crowther, P. A., Fullerton, A. W., & Hillier, D. J. 2004, *ApJ*, 610, 1021
- Esteban, C., & Fernández, M. 1998, *MNRAS*, 298, 185
- Farrenq, R., Guelachvili, G., Sauval, A. J., Grevesse, N., & Farmer, C. B. 1991, *J. Mol. Spectrosc.*, 149, 375
- Geballe, T. R., & Persson, S. E. 1987, *ApJ*, 312, 297
- Gummersbach, C. A., Zickgraf, F.-J., & Wolf, B. 1995, *A&A* 302, 409
- Hanson, M. M., Howarth, I. D., & Conti, P. S. 1997, *ApJ*, 489, 698
- Hartmann, L., Jaffe, D., & Huchra, J. P. 1980, *ApJ*, 239, 905
- Hillenbrand, L. A., Strom, S. E., Vrba, F. J., & Keene, J. 1992, *ApJ*, 397, 613
- Hillier, D. J., Lanz, T., Heap, S. R., et al. 2003, *ApJ*, 588, 1039
- Hofmann, K.-H., Balega, Y., Ikhsanov, N. R., Miroshnichenko, A. S., & Weigelt, G. 2002, *A&A*, 395, 891
- Hynes, R. I., Clark, J. S., Barsukova, E. A., et al. 2002, *A&A*, 392, 991
- Ignace, R., & Gayley, K. G. 2005, The nature and evolution of disks around hot stars (San Francisco: ASP), ASP Conf. Ser., 337
- Kastner, J. H., Buchanan, C. L., Sargent, B., & Forrest, W. J. 2006, *ApJ*, 638, L 29
- Kraus, M. 1997, CO band emission from a rotating disk, Diploma thesis, University of Bonn
- Kraus, M. 2000, Modeling of the Near IR Emission from the Peculiar B[e] star MWC 349, PhD thesis, University of Bonn
- Kraus, M., & Borges Fernandes, M. 2005, in ASP Conf. Ser. 337, The nature and evolution of disks around hot stars, ed. R. Ignace & K. G. Gayley (San Francisco: ASP), 254
- Kraus, M., & Miroshnichenko, A. S. 2006, Stars with the B[e] Phenomenon, (San Francisco: ASP), ASP Conf. Ser. 355
- Kraus, M., Borges Fernandes, M., & de Araújo, F. X. 2007, *A&A*, 463, 627
- Kraus, M., Borges Fernandes, M., Andrade Pilling, D., & de Araújo, F. X. 2006, in ASP Conf. Ser. 355, Stars with the B[e] Phenomenon, ed. M. Kraus & A. S. Miroshnichenko (San Francisco: ASP), 163

- Kraus, M., Borges Fernandes, M., Kubát, J., & de Araújo, F. X. 2008, *A&A*, 487, 697
- Kraus, M., Krügel, E., Thum, C., & Geballe, T. R. 2000, *A&A*, 362, 158
- Lamers, H.J.G.L.M., & Pauldrach, A.W.A. 1991, *A&A* 244, L5
- Lamers, H. J. G. L. M., Nota, A., Panagia, N., Smith, L. J., & Langer, N. 2001, *ApJ*, 551, 764
- Lamers, H. J. G. L. M., Zickgraf, F.-J., de Winter, D., Houziaux, L., & Zorec, J. 1998, *A&A*, 340, 117
- Lopes, D. F., Damineli Neto, A., & de Freitas Pacheco, J. A. 1992, *A&A*, 261, 482
- Maeder, A. & Meynet, G. 2000, *ARA&A* 38, 143
- Machado, M. A. D., & de Araújo, F. X. 2003, *A&A*, 409, 665
- Magalhães, A. M. 1992, *ApJ* 398, 286
- Magalhães, A. M., Melgarejo, R., Pereyra, A., & Carciofi, A. C. 2006, in *ASP Conf. Ser. 355, Stars with the B[e] Phenomenon*, ed. M. Kraus & A. S. Miroshnichenko (San Francisco: ASP), 147
- McGregor, P. J., Hyland, A. R., & Hillier, D. J. 1988, *ApJ*, 324, 1071
- McGregor, P. J., Hyland, A. R., & McGinn, M. T. 1989, *A&A*, 223, 237
- Melgarejo, R., Magalhães, A. M., Carciofi, A. C. & Rodrigues, C. V. 2001, *A&A*, 377, 581
- Meynet, G., & Maeder, A. 2003, *A&A*, 404, 975
- Miroshnichenko, A. S., Bjorkman, K. S., Grosso, M., et al. 2005, *A&A*, 436, 653
- Miroshnichenko, A. S., Frémat, Y., Houziaux, L., et al. 1998, *A&AS*, 131, 469
- Miroshnichenko, A. S., Klochkova, V. G., Bjorkman, K. S., & Panchuk, V. E. 2002, *A&A*, 390, 627
- Miroshnichenko, A. S., Levato, H., Bjorkman, K. S., & Grosso, M. 2003, *A&A*, 406, 673
- Miroshnichenko, A. S., Levato, H., Bjorkman, K. S., et al. 2004, *A&A*, 417, 731
- Morris, P. W., Eenens, P. R. J., Hanson, M. M., Conti, P. S., & Blum, R. D. 1996, *ApJ*, 470, 597
- Najita, J., Carr, J. S., Glassgold, A. E., Shu, F. H., & Tokunaga, A. T. 1996, *ApJ*, 462, 919
- Oudmajer, R. D., Proga, D., Drew, J. E., & de Winter, D. 1998, *MNRAS*, 300, 170
- Pelupessy, I., Lamers, H.J.G.L.M., & Vink, J.S. 2000, *A&A* 359, 695
- Pinsonneault, M. 1997, *ARA&A*, 35, 557
- Porter, J. M. 2003, *A&A*, 398, 631
- Schaller G., Schaerer D., Meynet G., Maeder A., 1992, *A&AS*, 96, 269
- Scoville, N. Z., Krotkov, R., & Wang, D. 1980, *ApJ*, 240, 929
- Searle, S. C., Prinja, R. K., Massa, D., & Ryans, R. 2008, *A&A*, 481, 777
- Tatulli, E., Malbet, F., Ménard, F., et al. 2008, *A&A*, 489, 1151
- Thi, W. F., van Dalen, B., Bik, A., & Waters, L. B. F. M. 2005, *A&A*, 430, L 61
- Winkler, H., & Wolf, B. 1989, *A&A*, 219, 151
- Wolf, B., & Stahl, O. 1985, *A&A*, 148, 412
- Waters, L. B. F. M. 2006, in *ASP Conf. Ser. 355, Stars with the B[e] Phenomenon*, ed. M. Kraus & A. S. Miroshnichenko (San Francisco: ASP), 87
- Waters, L. B. F. M., & Waelkens, C. 1998, *ARA&A*, 36, 233
- Zickgraf, F.-J. 2000, in *ASP Conf. Ser. 214, The Be Phenomenon in early-type stars*, ed. M. A. Smith, H. F. Henrichs & J. Fabregat (San Francisco: ASP), 26
- Zickgraf, F.-J. 2006, in *ASP Conf. Ser. 355, Stars with the B[e] Phenomenon*, ed. M. Kraus & A. S. Miroshnichenko (San Francisco: ASP), 135
- Zickgraf, F.-J., & Schulte-Ladbeck, R. E. 1989, *A&A*, 214, 274
- Zickgraf, F.-J., Wolf, B., Stahl, O., & Humphreys, R. M. 1989, *A&A*, 220, 206
- Zickgraf, F.-J., Wolf, B., Stahl, O., Leitherer, C., & Appenzeller, I. 1986, *A&A*, 163, 119
- Zickgraf, F.-J., Wolf, B., Stahl, O., Leitherer, C., & Klare, G. 1985, *A&A*, 143, 421
- Zickgraf, F.-J., Humphreys, R. M., Lamers, H. J. G. L. M., et al. 1996, *A&A*, 315, 510

List of Objects

‘GG Car’ on page 7